Metal-semiconductor and magnetic transitions in compensated polycrystalline $La_{1-x}Ca_xMnO_{3-\delta}$ ($x=0.20,0.25$)

T. L. Aselage,[1] D. Emin,[2] S. S. McCready,[1] E. L. Venturini,[1] M. A. Rodriguez,[1] J. A. Voigt,[1] and T. J. Headley[1]
[1]*Sandia National Laboratories, Albuquerque, New Mexico 87185-0613, USA*
[2]*Department of Physics and Astronomy, University of New Mexico, Albuquerque, New Mexico 87131-1156, USA*
(Received 7 April 2003; revised manuscript received 2 July 2003; published 27 October 2003)

The structures, magnetizations, conductivities, and Seebeck coefficients of single-phase polycrystalline $La_{0.75}Ca_{0.25}MnO_{3-\delta}$ and $La_{0.80}Ca_{0.20}MnO_{3-\delta}$ samples have been investigated as a function of the oxygen-vacancy concentration. Electrons from oxygen vacancies compensate holes introduced by Ca cations. Thus, by altering the oxygen deficiency δ the carrier concentration is changed while the calcium concentration remains constant. The effects of carrier and calcium concentrations on transport and magnetism are thereby separated from one another. We find the conductivity to be very sensitive to oxygen vacancies while the magnetization is not. In particular, oxygen vacancies decrease the conductivity and can eliminate low-temperature metal-like conduction. Thus ferromagnetism in $La_{0.75}Ca_{0.25}MnO_{3-\delta}$ and $La_{0.80}Ca_{0.20}MnO_{3-\delta}$ can occur without the concomitant occurrence of metallic conduction. However, electronic properties are sensitive to magnetic order. In particular, the temperature dependence of the Seebeck coefficient changes at the Curie temperature. These results are consistent with Jonker's suggestion that ferromagnetism in these manganites is induced by dopant-induced strains rather than by dopant-induced charge carriers. Loss of magnetic order fosters mobile charge carriers' collapse to localized dopant-related polaron states. Thus, the magnetically induced metal-semiconductor transitions in doped manganites are analogous to those of suitably doped ferromagnetic EuO.

DOI: 10.1103/PhysRevB.68.134448 PACS number(s): 75.47.Lx, 71.38.-k

I. INTRODUCTION

Undoped stoichiometric $LaMnO_3$ is an insulator whose Mn^{3+} magnetic moments order antiferromagnetically.[1] By contrast, the Mn magnetic moments order ferromagnetically when divalent alkaline-earth atoms ($A=$Ca, Sr, Ba) are substituted for trivalent La atoms.[2–4] The Curie temperatures T_C of these ferromagnets depend strongly on the size of the alkaline-earth atoms.[3]

These substitutions also alter these materials' electronic properties. In particular, electrical conductivities in $La_{1-x}A_xMnO_3$ increase with increasing x as hole-like charge carriers are introduced by the substitution of divalent alkaline-earth cations for La^{3+}. Below their Curie temperatures, the conductivities fall with increasing temperature. By contrast, above their Curie temperatures, the conductivities rise with increasing temperature. In this high-temperature regime the holes move by thermally activated hopping.[4–7] In particular, the very low ($\ll 1$ cm^2/V sec) and thermally activated Hall mobility is described as adiabatic hopping of small polarons.[8] The transition from a metal-like temperature dependence below T_C to a semiconductor-like temperature dependence above T_C produces a minimum of the conductivity near T_C.[3,4]

This metal-semiconductor transition shifts to higher temperatures with the application of a magnetic field.[4,9,10] The magnetic-field induced conversion of semiconducting transport to metallic transport produces negative magnetoresistance at temperatures near the metal-semiconductor transition.[4,9,10] This effect is now called colossal magnetoresistance.[9,10]

The near confluence of the metal-semiconductor and the ferromagnet-paramagnet transitions indicates a relationship between charge transport and alignment of the magnetic moments of Mn ions in $La_{1-x}A_xMnO_3$. This paper addresses the nature of this relationship.

Charge transport and magnetic order are linked through the combined effect of two phenomena.[11] First, exchange interactions foster alignment between a carrier's magnetic moment and a solid's local magnetic moments. Second, a carrier's transfer between sites is maximized if it maintains its spin orientation in the transfer.[12–14]

As a result, charge transport can be dramatically affected by magnetic ordering of the underlying lattice. For example, a large metal-semiconductor transition occurs near the Curie temperature in suitably doped EuO, a ferromagnetic insulator.[15,16] This metal-insulator transition is described as occurring when thermally induced misorientations of Eu^{2+} ions' $S=7/2$ magnetic moments induces the collapse of freely moving charge carriers into small polarons.[17,18] Since an applied magnetic field fosters parallel spin alignment of Eu^{2+} magnetic moments it increases the temperature of this metal-semiconductor transition. The increase of the transition temperature with applied magnetic field thereby produces what would now be termed colossal magnetoresistance.[19]

Charge carriers can also induce ferromagnetic alignment of local magnetic moments. In particular, if the intersite exchange of an antiferromagnet is weak enough, a carrier can induce parallel alignment of associated magnetic moments. This carrier-induced local ferromagnetic cluster in a semiconductor is termed a *magnetic polaron*.[20] Magnetic polarons, while not common, are reported in weak (low Néel temperature) antiferromagnets (e.g., EuTe).[11,20] A sufficient density of carriers can even induce formation of a global ferromagnet.[20]

Most magnetic insulators order as antiferromagnets.[11] Furthermore, most antiferromagnetic insulators retain their antiferromagnetic ordering when doped.[21,22] Lanthanum manganite is unusual. The magnetic ordering of $LaMnO_3$ changes from antiferromagnetic to ferromagnetic upon doping with divalent ions. This exceptional behavior has been cited as indicative of carrier-induced ferromagnetism.[12–14,23,24]

Three specific observations cast doubt on this attribution. In particular, Jonker noted that $LaMnO_3$ is an unusual antiferromagnet.[22] Its manifestation of Curie-Weiss behavior in its paramagnetic phase presages ferromagnetic, rather than antiferromagnetic, ordering. Antiferromagnetic ordering may result from the symmetry-lowering structural change that accompanies magnetic ordering. Impeding this structural transformation with dopant atoms may account for the dopant-induced ferromagnetism.[22]

Second, the strength of carrier-induced ferromagnetism is expected to rise with the carrier density. However, the Curie temperature is found to depend strongly on the size of divalent dopants rather than on their density.[22,25,26]

Third, carrier-induced ferromagnetism is expected to disappear as carriers are removed. However, compensating holes from divalent-dopants with electrons from oxygen vacancies has little affect on the ferromagnetism. Compensated materials remain ferromagnetic with only a slight decrease in Curie temperature.[27–29] Meanwhile, consistent with effective compensation, the conductivities of samples fall sharply as oxygen vacancies are introduced.[27–30] Even uncompensated samples with moderate calcium doping ($La_{0.82}Ca_{0.18}MnO_3$) are both ferromagnetic and insulating.[31]

In this paper, we report measurements of the structures, magnetizations, conductivities, and Seebeck coefficients of compensated lanthanum manganites $La_{0.75}Ca_{0.25}MnO_{3-\delta}$ and $La_{0.80}Ca_{0.20}MnO_{3-\delta}$. Compensation is very effective in decreasing the conductivity. As a result, compensation produces single-phase samples that are both ferromagnetic and semiconducting. Thus, metallic conduction is not a prerequisite for these materials' ferromagnetism. However, the underlying magnetic order does affect electronic carriers and their motion. In particular, Seebeck coefficients undergo a transition at the Curie temperature.

II. EXPERIMENTAL DETAILS

A coprecipitation process was used to produce powders of $La_{0.80}Ca_{0.20}MnO_3$ and of $La_{0.75}Ca_{0.25}MnO_3$. The powders were then pressed and sintered to form bulk samples. Controlled concentrations of oxygen vacancies were introduced by annealing bulk samples in an ambient with a fixed partial oxygen pressure. Magnetization, conductivity and Seebeck coefficient measurements were made on these samples.

A. Sample preparation

To begin, aqueous metal nitrate solutions of the desired cation stoichiometry were prepared by mixing appropriate stock solutions. The lanthanum stock solution was prepared by dissolving La_2O_3 (Aldrich, 99.999%) in high purity, concentrated HNO_3 (Fisher, Optima). The lanthanum content of the La_2O_3 was corrected for carbonate and/or hydroxide adsorption by gravimetric assay, determined by measuring the change in mass of as-received La_2O_3 after heating in air at 1000 °C for 6 h. The manganese stock solution was prepared by dissolving hydrated manganese nitrate (Alfa Aesar, 99.98%) in water. The manganese content of the as-received nitrate was determined gravimetrically by conversion to Mn_3O_4 by heating in air at 1200 °C for 6 h.[32] Calcium carbonate (Aldrich, 99.999%) was dissolved using high purity nitric acid to form the calcium stock solution.

Powders having the desired stoichiometry were prepared by mixing an aqueous solution of metal nitrates with a precipitant, an ammonium carbonate solution. The ammonium carbonate (Fisher, ACS) concentration of the precipitant solution was adjusted such that the final pH after addition of the metal nitrate solution was between 8 and 9 to assure complete precipitation.[29]

The metal nitrate solution was pumped directly into the mixing head of a high-shear mixer placed in the precipitant solution. This rapid mixing procedure ensured a homogenous cation distribution in the ultimate powders.

The precipitate slurry was vacuum filtered, air-dried at 60 °C, and calcined in air at 1000 °C for 3 h. The nonmetal ions of the aqueous solutions (nitrate, ammonium, and carbonate) were chosen to leave no residues in the powders after calcination. X-ray diffraction of the calcined powders only found evidence of the $La_{1-x}Ca_xMnO_3$ perovskite structure.

Calcined powders were pressed into pellets of several mm thickness and approximately 1.9 cm diameter under isostatic pressure of 28 000 psi. Pellets were sintered at 1350 °C for 2 h in flowing O_2, then cooled slowly to room temperature. The density of each of the sintered pellets was near 6 g/cm^3, about 95% of the theoretical density. Rectangular bars of approximate dimension 0.2 cm×0.2 cm×1.0 to 1.8 cm were cut from the pellets for transport measurements. Samples for magnetization measurements were of similar cross section and between 0.3 and 0.4 cm in length. Powder samples of each composition were obtained by grinding a portion of the sintered pellets.

Powder x-ray diffraction patterns were obtained with a Siemans D500 $\theta/2\theta$ diffractometer using Cu $K\alpha$ radiation. Data were collected from 15° to 125° 2θ in 0.05° steps at 22 s per step. X-ray diffraction confirmed that all as-sintered samples were single phase. Rietveld refinements of Ca/La site occupancies were consistent with the specified compositions $x=0.20$ or $x=0.25$. Electron probe microanalysis also confirmed samples' cation ratios.

The oxygen contents of as-sintered samples, $3-\delta$ in $La_{1-x}Ca_xMnO_{3-\delta}$, were calculated to within ± 0.002 from the release of gaseous oxygen when samples decompose in flowing 10% H_2/90% N_2 at 1200 °C according to the chemical formula

$$La_{1-x}Ca_xMnO_{3-\delta} \rightarrow \left(\frac{1-x}{2}\right)La_2O_3 + (1+x)Ca_{x/1+x}Mn_{1/1+x}O + \left(\frac{1+x-2\delta}{4}\right)O_2. \quad (1)$$

TABLE I. Summary of sample data.

Sample composition x in $La_{1-x}Ca_xMnO_{3-\delta}$	$P(O_2)$ (atm)	Oxygen deficit δ in $La_{1-x}Ca_xMnO_{3-\delta}$	a (Å)	b (Å)	c (Å)	Cell volume (Å^3)	T_C (K)	N_B, Bohr magnetons per formula unit at saturation 5 K
0.25	1[a]	0.011	5.481	7.748	5.495	233.39	221,[c] 221[d]	3.7,[c] 3.9[d]
0.25	10^{-4}	0.011	5.482	7.751	5.497	233.58	208[c]	3.8[c]
0.25	$10^{-7.8}$	0.04	5.482	7.753	5.500	233.80	187[d]	3.6[d]
0.25	10^{-9}[b]	0.20[b]	5.631[b]	7.718[b]	5.528[b]	240.2[b]	123[c]	1.8[c]
0.20	1[a]	0.002	5.490	7.760	5.504	234.49	192,[e] 194[f]	3.9,[e] 3.7[f]
0.20	10^{-4}	0.02	5.496	7.767	5.505	235.03	188[e]	3.9[e]
0.20	10^{-5}	0.02	5.497	7.768	5.505	235.05	189[e]	3.9[e]
0.20	$10^{-7.2}$	0.04	5.500	7.774	5.505	235.39	176[e]	3.6[e]
0.20	$10^{-7.8}$	0.08	5.514	7.777	5.512	236.40	163[e]	3.4[e]
0.20	10^{-9}[b]	0.15[b]	5.623[b]	7.723[b]	5.525[b]	239.95[b]	122[f]	1.7[f]
0.20	10^{-9}, then re-anneal at 1 atm		5.480	7.748	5.503	233.63	194[f]	3.8[f]

[a]Values listed for $P(O_2)=1$ atm were obtained from the as-sintered samples.

[b]X-ray powder diffraction finds samples equilibrated at $P(O_2)$ of 10^{-9} atm to be a two-phase mixture of the orthorhombic manganite phase and $Ca_yMn_{1-y}O$. The lattice constants of the cubic $Ca_yMn_{1-y}O$ solid solution, 4.617 Å for the $x=0.20$ sample and 4.635 Å for the $x=0.25$ sample, suggest that y is approximately 0.50.

[c,d]Used to denote which of two samples was used in the magnetization measurement for $x=0.25$.

[e,f]Used to denote which of two samples was used in the magnetization measurement for $x=0.20$.

The O_2 loss was determined thermogravimetrically by weighing the solid reaction products, La_2O_3 and the mixed crystal $Ca_{x/1+x}Mn_{1/1+x}O$. This procedure relies on the well-established trivalence of La and the divalence of Mn under these reducing conditions.[34] X-ray diffraction of the solid reduction products confirmed that only La_2O_3 and $Ca_{x/1+x}Mn_{1/1+x}O$ were present. Furthermore, the lattice constants measured for cubic $Ca_{x/1+x}Mn_{1/1+x}O$ ($a=4.505$ Å for $x=0.20$ and $a=4.516$ Å for $x=0.25$) are very close to those predicted with the linear dependence of a on x for $0\leqslant x\leqslant 1$ ($a=4.506$ Å for $x=0.20$ and 4.518 Å for $x=0.25$) of Vegard's law.

B. Vacancies

Oxygen vacancies were then introduced and controlled by annealing as-sintered samples at 1200 °C in an ambient of fixed oxygen partial pressure $P(O_2)$. Bulk samples for magnetization, transport, and powder for x-ray diffraction were annealed simultaneously. $P(O_2)$ levels between 10^{-4} and 10^{-5} atm, confirmed by a stabilized-zirconia oxygen sensor, were supplied in premixed Ar/O_2 mixtures. $P(O_2)$ levels between 10^{-7} and 10^{-9} atm, were established through the CO/CO_2 equilibrium at 1200 °C, where flows of CO and CO_2 were independently metered and controlled with a total flow rate of about 50 sccm. After a minimum of 48 h at 1200 °C, samples were cooled rapidly (to below 500 °C within two minutes) in an actively cooled portion of an Al_2O_3 tube within the furnace. When CO/CO_2 mixtures were in use, the gas flow was switched to high-purity Ar immediately after removing samples to the cold end of the chamber. Oxygen deficiencies were then calculated to within ± 0.01 from samples' mass loss.

C. Magnetic and electrical measurements

Magnetic measurements were made using a Quantum Design SQUID magnetometer. Electrical conductivities were measured using a standard four-point technique with sputtered Ag contacts. Seebeck coefficients were measured on the same samples by clamping samples' ends within large Cu blocks whose independently controlled temperatures were slowly swept through differences of up to ± 3 K. The Cu-block temperatures were measured with Cernox resistance thermometers, chosen for their very small sensitivity to magnetic field.

III. EXPERIMENTAL RESULTS

Oxygen deficits of up to $\delta\approx 0.8$ are introduced without producing significant phase separation. The Curie temperature T_C falls slowly ($\leqslant 10\%$ for $x=0.2$) with increasing deoxygenation before falling sharply upon phase separation. By contrast, the electrical conductivity falls sharply with increasing oxygen deficiency. The conductivity then maintains its semiconducting behavior through T_C. Nonetheless, the temperature dependence of the Seebeck coefficient changes at T_C. Thus, the semiconductor's Seebeck coefficient is affected by magnetic order.

A. Deoxygenation and phase separation

Table I shows the oxygen deficit, δ in $La_{1-x}Ca_xMnO_{3-\delta}$, for samples with $x=0.20$ and $x=0.25$ as a function of the $P(O_2)$ of their 1200 °C anneal. The dependence of δ on $P(O_2)$ at 1200 °C is in very good agreement with earlier measurements.[35,36]

X-ray powder diffraction patterns were obtained as func-

tions of the oxygen partial pressure. Patterns for $La_{0.8}Ca_{0.2}MnO_{3-\delta}$ are shown in Fig. 1. Similar diffraction patterns were obtained for $La_{0.75}Ca_{0.25}MnO_{3-\delta}$ samples. Extra peaks, denoted by asterisks, emerge at very low oxygen partial pressure $P(O_2)=10^{-9}$ atm. These additional peaks indicate that samples decompose when the oxygen deficit becomes too great. Earlier investigations did not mention this decomposition.[34,35]

Lattice constants for single-phase samples are only slightly affected by deoxygenation. By contrast, large shifts of lattice constants result at very low oxygen partial pressure $P(O_2)=10^{-9}$ atm. Table I lists the dimensions of samples' orthorhombic unit cells. Here $a\approx c\approx\sqrt{2}a_p$ and $b\approx 2a_p$, where a_p is the dimension (≈ 3.9 Å) of the parent cubic perovskite cell.

X-ray diffraction results suggest that samples with excess oxygen depletion decompose into two phases. The decomposition is approximately described by the chemical formula

$$La_{1-x}Ca_xMnO_{3-\delta}\rightarrow 2y(Ca_{0.5}Mn_{0.5}O)+(1-y)[La_{(1-x)/(1-y)}Ca_{(x-y)/(1-y)}MnO_{(3-\delta-2y)/(1-y)}]. \quad (2)$$

Here the equal concentrations of Ca and Mn in the $Ca_zMn_{1-z}O$ solid solution were inferred from the value of the lattice constants for this phase. The residual perovskite phase contains a higher oxygen concentration and a lower Ca concentration than its antecedent since $3>(3-\delta-2y)/(1-y)>(3-\delta)$ and $0<(x-y)/(1-y)<x$ when $\delta<y<x<1$. The lattice constants given in Table I for the decomposed samples are consistent with the residual perovskite having a small Ca concentration.[1,22] The large orthorhombic distortion of the residual perovskite's unit cell produces the (101)-(020) splitting that is evident in Fig. 1 for the decomposed material.

Transmission electron microscopy (TEM) was used to examine two $La_{0.8}Ca_{0.2}MnO_{3-\delta}$ samples: the as-sintered sample and the sample annealed at $P(O_2)=10^{-7.8}$ atm. Microstructural features resemble those reported by others.[37–39] Energy dispersive spectroscopy (EDS) found both samples' compositions to be homogeneous over the beams' length scale, roughly 500 Å.

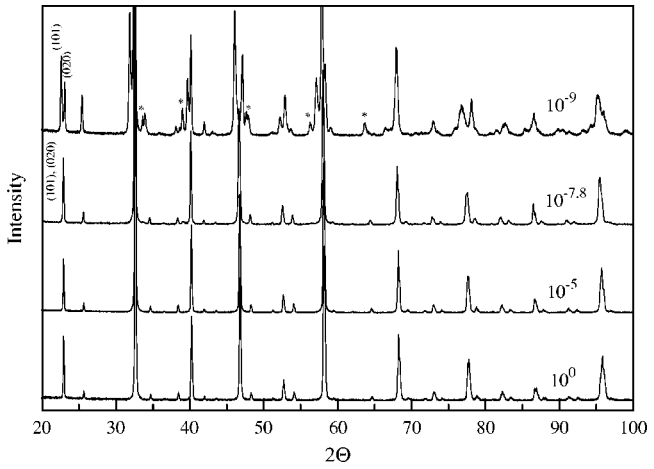

FIG. 1. X-ray powder diffraction patterns of four samples of $La_{0.8}Ca_{0.2}MnO_{3-\delta}$ are labeled by the oxygen partial pressure $P(O_2)$ used in deoxygenating anneals. Indicative of single-phase material, each reflection in the lower three patterns $P(O_2)\geq 10^{-7.8}$ atm, can be indexed with an orthorhombic unit cell of a perovskite. By contrast, the uppermost pattern illustrates a phase-separated sample. Its pattern contains reflections of a decomposition product $Ca_yMn_{1-y}O$ with $y\approx 0.5$, denoted by asterisks. The top pattern also contains peaks from the other decomposition product, a Ca-depleted perovskite. The splittings of the (101)-(020) reflections result from the increased orthorhombic distortion of this decomposition product.

Many grains of the as-sintered sample contain a high density of fine domains. Single-domain diffraction patterns were rarely observed. Rather, electron diffraction patterns indicated overlapping domains rotated by 45° with respect to one another. Antiphase domain boundaries were also seen in many grains. Domain fragmentation and antiphase boundaries were also observed, with generally larger domain sizes, in the sample annealed at $P(O_2)=10^{-7.8}$ atm.

TEM examination of the $La_{0.8}Ca_{0.2}MnO_{3-\delta}$ sample annealed at $P(O_2)=10^{-7.8}$ atm found occasional small inclusions of $Ca_yMn_{1-y}O$. This observation suggests incipient decomposition, phase separation undetected by x-ray diffraction. Thus, we take the oxygen deficiency produced when annealing with $P(O_2)=10^{-7.8}$ atm to be the limit for single-phase material.

B. Magnetization

Magnetization of $La_{0.8}Ca_{0.2}MnO_{3-\delta}$ and $La_{0.75}Ca_{0.25}MnO_{3-\delta}$ are plotted against temperature in Fig. 2 for samples annealed in different deoxygenating environments, denoted by their oxygen partial pressure $P(O_2)$. The onset of ferromagnetism is relatively sharp in all single-phase samples $P(O_2)\geqslant 10^{-7.8}$ atm. The Curie temperatures, listed in Table I, of single-phase samples decrease only slightly as the oxygen deficiency increases.

Magnetization measurements confirmed that each single-phase sample could be fully magnetized. As shown by the examples in Fig. 3, the magnetization at 5 K approaches ferromagnetic saturation at $H\leqslant 10$ kOe. The saturation values, presented in Table I, are expressed as the magnetization per formula unit. Saturation is close to that expected from full ferromagnetic alignment of each Mn *d* electron, 3.8 to 3.9 Bohr magnetons per formula unit depending on the Ca dopant and O vacancy concentrations. The saturation magnetization measurements depicted in Fig. 3 were also performed at 125 K. The fractional decline in the saturation magnetization of the as-sintered sample is smaller than that of the deoxygenated sample. This effect may be attributed

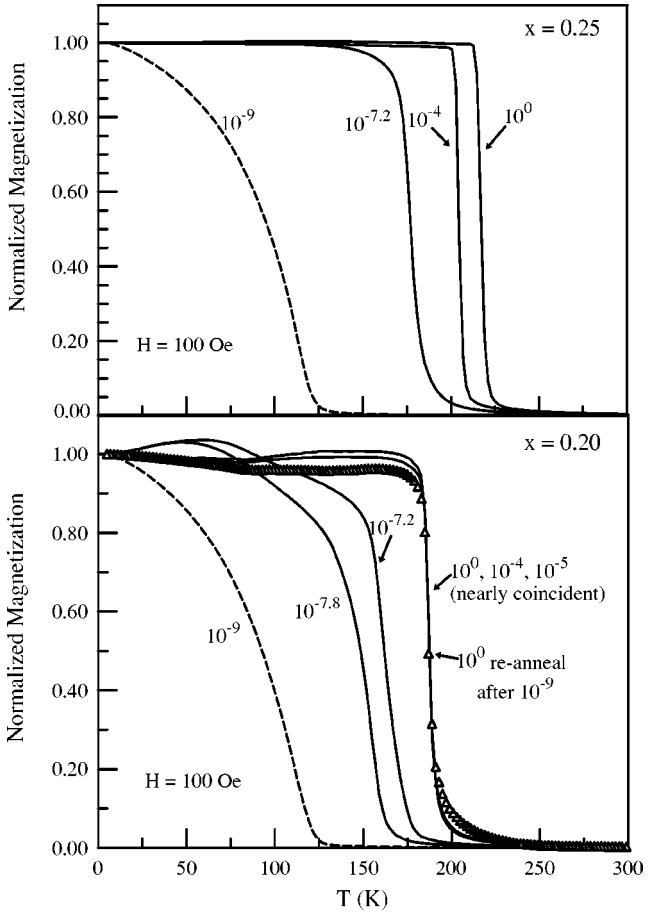

FIG. 2. The normalized magnetization $M(T)/M(5\,\mathrm{K})$, measured upon cooling from room temperature to 5 K in a field of 100 Oe, is plotted versus temperature for $La_{1-x}Ca_xMnO_{3-\delta}$ with $x=0.25$ (top) and 0.20 (bottom). Curves are labeled by the oxygen partial pressure $P(O_2)$ used in deoxygenating anneals. The dashed curves indicate results for phase-separated samples. Open triangles denote measurements of a phase-separated sample that was reoxidized by annealing at $P(O_2)=1$ atm.

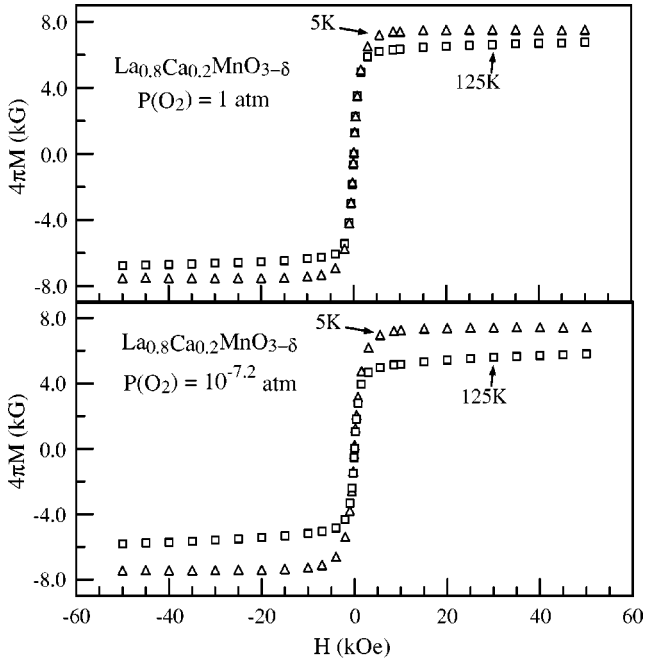

FIG. 3. The magnetization is plotted versus applied field for $La_{0.8}Ca_{0.2}MnO_{3-\delta}$ samples at 5 and 125 K. The upper panel shows the magnetization of an as-sintered sample, annealed at 1200 °C at standard oxygen partial pressure $P(O_2)=1$ atm. The lower panel shows the magnetization of a deoxygenated sample produced by annealing at 1200 °C in a reduced oxygen partial pressure $P(O_2)=10^{-7.8}$ atm.

solely to the Curie temperature of the as-sintered sample, $T_C=192$ K, being higher than that of the deoxygenated sample $T_C=176$ K.

Decomposed samples, dashed curves of Fig. 2, have relatively low Curie temperatures, and manifest broad transitions that are difficult to saturate. Such behavior characterizes weak ferromagnetism resulting from canted spin arrangements. Such ferromagnetism is strongest in $La_{1-x}Ca_xMnO_3$ for small x, although canted ferromagnetism is reported for x as large as 0.20.[40] Similar behavior has been reported in Sr- and Ba-doped lanthanum manganites.[41,42] Since the residual perovskite phase of decomposed samples is depleted in Ca, this phase may account for the weak ferromagnetism of decomposed samples.

A decomposed sample of $La_{0.8}Ca_{0.2}MnO_{3-\delta}$ was reoxidized at 1200 °C and 1 atm of O_2. Structural and magnetic data for this reoxidized sample are contained in the final column of Table I and depicted by the triangular symbols in the lower panel of Fig. 2. These properties of the reoxygenated sample were restored to near those of material that was never deoxygenated. This experiment illustrates the reversibility of the deoxygenation process.

C. Electrical transport

The dc conductivities of single-phase $La_{1-x}Ca_xMnO_{3-\delta}$ with $x=0.20$ and 0.25 are plotted against reciprocal temperature $1/T$ in Fig. 4. Each plot is labeled with the partial pressure of oxygen used is the sample's annealing. Arrows denote the Curie temperatures of each sample. The conductivities and Seebeck coefficients of our 1350 °C-sintered samples closely resemble those of similar samples prepared at comparably high temperatures.[33]

The conductivities are always well below the minimum metallic conductivity, $e^2/\hbar a \approx 10^3(\mathrm{Ohm\,cm})^{-1}$.[43] At the highest temperatures the conductivities are nearly thermally activated, $\sigma \approx \sigma_0 \exp(-E/kT)$, where the extrapolated values σ_0 are of the order of 10^3 $(\mathrm{Ohm\,cm})^{-1}$. This value of σ_0 is comparable to that typical of adiabatic multiphonon hopping between sites whose average separation is s, $e^2\nu/skT$, where ν is the characteristic vibration frequency.[44] The activation energies 0.1–0.2 eV increase monotonically with oxygen deficiency with the exception of the sample with $x=0.25$ and $P(O_2)=10^{-7.8}$ atm that has an unexpectedly small activation energy.

The effects of deoxygenating anneals on samples' conductivities were reproducible and roughly reversible. For example, the conductivities of two different samples of $La_{0.75}Ca_{0.25}MnO_{3-\delta}$ annealed with $P(O_2)=10^{-4}$ atm lie

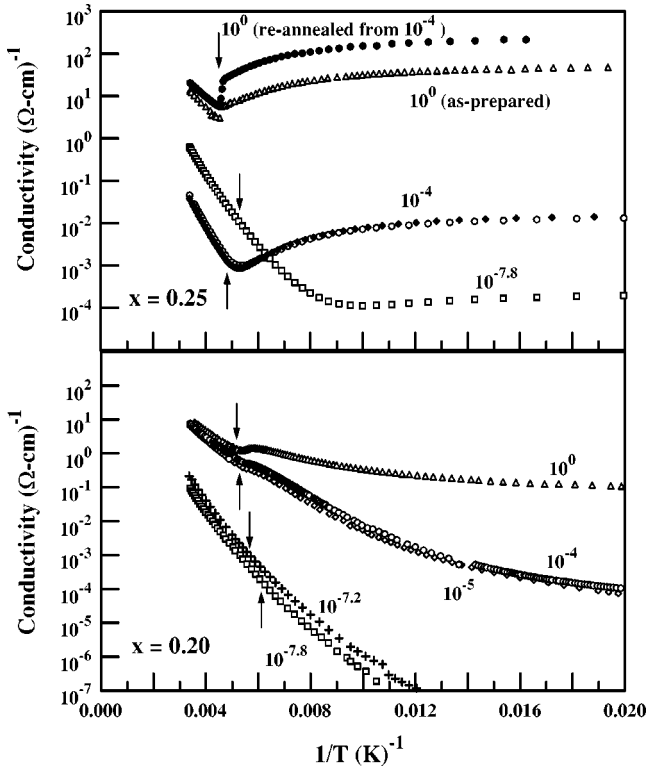

FIG. 4. Conductivities of $La_{1-x}Ca_xMnO_{3-\delta}$ for $x=0.20$ and 0.25 are plotted separately against reciprocal temperature for as-sintered samples and those annealed in different deoxygenating environments. The deoxygenating environment is defined by the oxygen partial pressure during annealing. The Curie temperature of each sample is indicated with an arrow. The conductivity of a sample that was first deoxygenated with $P(O_2)=10^{-4}$ atm and then reoxygenated is also shown.

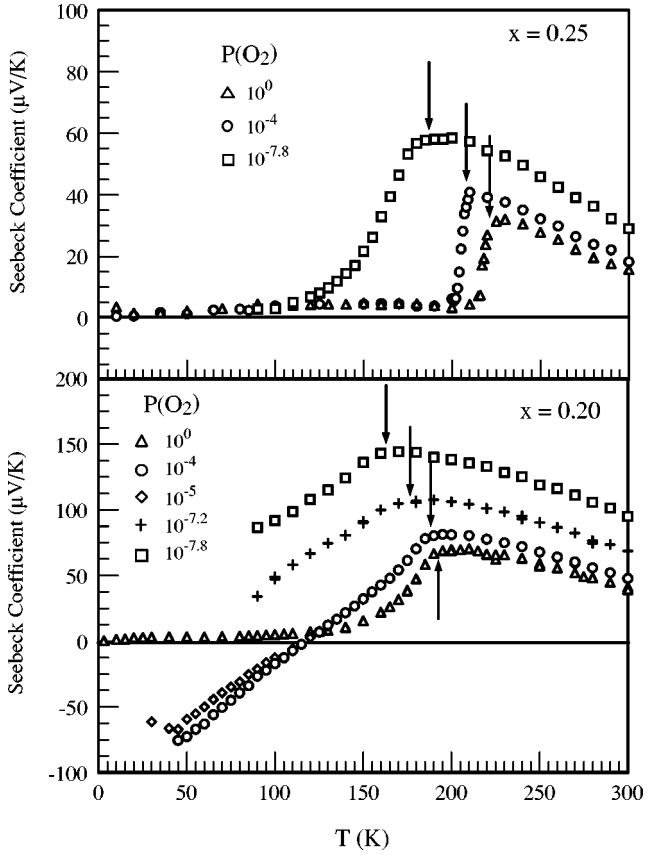

FIG. 5. Seebeck coefficients of $La_{1-x}Ca_xMnO_{3-\delta}$ for $x=0.20$ and 0.25 are plotted separately against temperature for samples annealed in different deoxygenating environments. The deoxygenating environment is defined by the oxygen partial pressure during annealing. The Curie temperature of each sample is indicated with an arrow. Note the difference in scale between the upper panel $x=0.25$ and the lower panel $x=0.20$.

nearly on top of one another. Furthermore, reoxygenating one of these samples [for 48 h at 1200 °C and $P(O_2)=1$ atm] resulted in a conductivity that resembles that of an as-sintered sample.

The conductivity of a semiconducting sample [$x=0.20$, $P(O_2)$ of $10^{-7.2}$ atm] was measured as a function of applied magnetic field between 100 and 300 K. Neither the magnitude nor the temperature dependence of the conductivity were altered by fields as large as 8 T.

The Seebeck coefficients of single-phase samples of $La_{1-x}Ca_xMnO_{3-\delta}$ are plotted against temperature in Fig. 5. An arrow indicates the Curie temperature of each sample. The sign of the Seebeck coefficient indicates the sign of the predominant carrier. In addition, the magnitude of the Seebeck coefficient typically falls as the carrier density rises. Thus, these results of Fig. 5 imply that the predominant carriers are holes whose density tends to rise with Ca content and fall with deoxygenation. In one insulating deoxygenated sample the Seebeck coefficient even manifests a negative sign at low-enough temperatures $T<120$ K. In other words, oxygen vacancies appear to compensate holes introduced by Ca substituting for La.

The temperature dependence of each Seebeck coefficient of Fig. 5 changes at the Curie temperature. Such changes are generally attributed to a metal-semiconductor transition that often accompanies the loss of long-range magnetic order at the Curie temperature. However, de-oxygenated samples show no indication of a metal-semiconductor transition at T_C. Indeed, Fig. 4 indicates the persistence of phonon-assisted hopping in sufficiently deoxygenated samples as the temperature is lowered below the Curie temperature. Thus, the change of the Seebeck coefficient that occurs near T_C is linked to the change of long-range magnetic order.

IV. DISCUSSION

Doped $La_{1-x}A_xMnO_3$, where A is a divalent cation (Ca, Sr, or Ba), has been the object of study for half a century. These materials are ferromagnets with metal-semiconductor transitions near their Curie temperature. It has long been established that charge carriers in the high-temperature semiconducting phase move by thermally assisted (small-polaron-like) hopping.[4–6,27]

An outstanding issue has been to understand the relationship between the magnetic and transport transitions. In particular, do the delocalized charge carriers of the low-temperature metallic phase induce the material's ferromagnetism? An alternative possibility is that these ma-

terials are ferromagnets in the absence of charge carriers. Then in appropriate circumstances the change of magnetic order can induce the material's carriers to undergo a metal-semiconductor transition.

To address this issue, we have studied the effects of deoxygenation on the magnetic, electronic and thermal properties of $La_{1-x}Ca_xMnO_3$. The introduction of oxygen vacancies tends to compensate charge carriers and further disorder the material. Will the linkage between the magnetic and transport transitions survive with deoxygenation?

We find that deoxygenation separates the magnetic and transport transitions. The Curie temperatures of single-phase, fully saturated ferromagnets change little with deoxygenation. However, deoxygenation causes these samples' electrical conductivity to fall sharply. De-oxygenated samples maintain small-polaron-like semiconductor behavior through their ferromagnetic transitions. Thus, ferromagnetism occurs without metallic conduction.

Nonetheless, magnetic order affects the charge carriers. In particular, the Seebeck coefficient, the entropy transport per carrier charge by a carrier, has a maximum at the Curie temperature.

A metal-semiconductor transition similar to that in doped-$LaMnO_3$ occurs for carriers added to a ferromagnetic insulator.[45] In particular, a metal-semiconductor transition and associated colossal magnetoresistance similar to those of doped $LaMnO_3$ occur when the ferromagnetic insulator EuO is doped to produce a suitable density of large-radius donors (about 1%).[15,16] Below the Curie temperature the overlap between donors is then sufficient to produce metallic impurity conduction. The metal-semiconductor transition that occurs near the Curie temperature has been described in terms of a donor-state collapse.[17] In particular, as the temperature is raised close to the Curie temperature the cost in entropy of having large-radius donor electrons align the local moments they contact becomes too great. The donors then collapse to severely localized small-polaron-like states. The smallness of the overlap between collapsed donors suppresses metallic conduction, thereby leading to semiconducting behavior above the Curie temperature. Colossal magnetoresistance results because the temperature of a donor-state collapse, and of the resultant metal-semiconductor transition, rises in an applied magnetic field.[18,19]

The doping levels in doped-$LaMnO_3$ are much too high for electronic transport to be as simple as in doped-EuO. In particular, the probability that none of the six La sites in the unit cells surrounding a Ca substitution also has a Ca substitution is small: $(1-x)^6=0.26$ for $x=0.20$ and $(1-x)^6=0.18$ for $x=0.25$. That is, there are few isolated dopants. Thus, holes introduced by Ca substitutions primarily exist and move on Mn ions within complexes containing many dopants.[5] Many of the holes introduced by Ca substitution will be bound within dopant complexes. In this situation only a fraction of these holes can hop relatively easily.

Deoxygenation further complicates this complex type of impurity conduction. Oxygen vacancies enhance the disorder while they serve as traps or sinks for holes. In this way de-oxygenation increases the activation energy of the conductivity. In addition, we find that less than 3% oxygen vacancies can significantly reduce the fraction of relatively mobile carriers, as indicated by the sensitivity of the Seebeck coefficient to deoxygenation. Such effective compensation occurs when deoxygenation significantly reduces the density of relatively mobile carriers. Because of their low carrier densities, effectively compensated strongly insulating samples are prone to ambipolar conduction. Ambipolar conduction may account for the ''anomaly'' in the sign of the low-temperature Seebeck coefficient of one sample shown in Fig. 5.

All told, entropy changes associated with the alignment of local moments linked to carriers drive their collapse in the vicinity of T_C. Anomalies in the Seebeck coefficient near T_C indicate carriers' collapse. The effect of carriers' collapse on the adiabatic hopping conductivity of deoxygenated samples is muted when hopping transport already predominates below T_C. Adiabatic small-polaronic hopping is governed by the energy landscape experienced by hopping carriers. Carriers' collapse alters the percolation paths that dominate the hopping conductivity.

ACKNOWLEDGMENTS

The authors thank P. F. Hlava for electron microprobe measurements and C. C. Collins and D. L. Sipola for laboratory assistance. The Division of Materials Science, Office of Basic Energy Sciences of the U.S. Department of Energy supported this work under Contract No. DE-AC04-94AL85000. Sandia is a multiprogram laboratory operated by Sandia Corporation, a Lockheed Martin Company.

[1] E. O. Wollan and W. C. Koehler, Phys. Rev. **100**, 545 (1955).
[2] G. H. Jonker and J. H. van Santen, Physica (Amsterdam) **XVI**, 337 (1950).
[3] J. H. van Santen and G. H. Jonker, Physica (Amsterdam) **XVI**, 599 (1950).
[4] J. Volger, Physica (Amsterdam) **XX**, 49 (1954).
[5] R. C. Miller, R. R. Heikes, and R. Mazelsky, J. Appl. Phys. **32**, 2202 (1961).
[6] M. Kertesz, I. Riess, D. S. Tannhauser, R. Langpape, and F. J. Rohr, J. Solid State Chem. **42**, 125 (1982).
[7] M. Jaime, H. Hardner, M. B. Salamon, M. Rubinstein, P. Dorsey, and D. Emin, Phys. Rev. Lett. **78**, 951 (1997).
[8] D. Emin and T. Holstein, Ann. Phys. (N.Y.) **53**, 439 (1969).
[9] S. Jin, T. H. Tiefel, M. McCormack, R. A. Fastnacht, R. Ramesh, and L. H. Chen, Science **264**, 413 (1994).
[10] A. P. Ramirez, W. Bao, and S.-W. Cheong, Phys. Rev. Lett. **75**, 3336 (1995).
[11] S. Methfessel and D. C. Mattis, *Magnetic Semiconductors in Zeitschrift fur Physik* (Springer-Verlag, Heidelberg, 1968), Vol. 18a, pp. 389–562.
[12] C. Zener, Phys. Rev. **82**, 403 (1951).
[13] P. W. Anderson and H. Hasegawa, Phys. Rev. **100**, 675 (1955).

[14] P.-G. deGennes, Phys. Rev. **118**, 141 (1960).
[15] J. B. Torrance, M. W. Shafer, and T. R. McGuire, Phys. Rev. Lett. **29**, 1168 (1972).
[16] C. Godart, A. Mauger, J. P. Desfours, and J. C. Achard, J. Phys. (France) **41**, C5-205 (1980).
[17] D. Emin, M. S. Hillery, and N.-L. H. Liu, Phys. Rev. B **35**, 641 (1987).
[18] M. S. Hillery, D. Emin, and N.-L. H. Liu, Phys. Rev. B **38**, 9771 (1988).
[19] M. R. Oliver, J. O. Dimmock, A. L. McWhorter, and T. B. Reed, Phys. Rev. B **5**, 1078 (1972).
[20] D. Emin and M. S. Hillary, Phys. Rev. B **37**, 4060 (1988).
[21] G. H. Jonker and J. H. van Santen, Physica (Amsterdam) **XIX**, 120 (1953).
[22] G. H. Jonker, Physica (Amsterdam) **XXII**, 707 (1956).
[23] A. J. Millis, P. B. Littlewood, and B. I. Shraiman, Phys. Rev. Lett. **74**, 5144 (1995).
[24] A. J. Millis, B. I. Shraiman, and R. Mueller, Phys. Rev. Lett. **77**, 175 (1996).
[25] L. Rodriguez-Martinez and J. P. Attfield, Phys. Rev. B **54**, 15 622 (1996).
[26] J. P. Attfield, Comput. Mater. Sci. **10**, 3239 (1998).
[27] J. Tanaka, M. Umehara, S. Tamura, M. Tsukioka, and S. Ehara, J. Phys. Soc. Jpn. **51**, 1236 (1982).
[28] I. O. Troyanchuk, L. V. Balyko, and G. L. Bychkov, Sov. Phys. Solid State **31**, 716 (1989).
[29] J. F. Mitchell, D. N. Argyriou, C. D. Potter, D. G. Hinks, J. D. Jorgensen, and S. D. Bader, Phys. Rev. B **54**, 6172 (1996).
[30] A. M. De Leon-Guevera, P. Berthet, J. Berthon, F. Millot, and A. Revcoleschi, J. Alloys Compd. **262–263**, 163 (1997).
[31] P. Schiffer, A. P. Ramirez, W. Bao, and S.-W. Cheong, Phys. Rev. Lett. **75**, 3336 (1995).
[32] J. Tanaka, K. Takahashi, Y. Yajima, and M. Tsukioka, Chem. Lett. **1982**, 1847 (1982).
[33] M. F. Hundley and J. J. Neumeier, Phys. Rev. B **55**, 11 511 (1997).
[34] A. Z. Hed and D. S. Tannhauser, J. Electrochem. Soc. **114**, 314 (1967).
[35] S. Tamura and A. Yamamoto, J. Mater. Sci. Lett. **15**, 2120 (1980).
[36] J. W. Stevenson, M. M. Nasrallah, H. U. Anderson, and D. M. Sparlin, J. Solid State Chem. **102**, 185 (1993).
[37] M. Hervieu, G. Van Tendeloo, V. Caignaert, A. Maignan, and B. Raveau, Phys. Rev. B **53**, 14274 (1996).
[38] O. I. Lebedev, G. Van Tendeloo, S. Amelinckx, B. Leibold, and H.-U. Habermeier, Phys. Rev. B **58**, 8065 (1998).
[39] M. Arao, Y. Koyama, Y. Inoue, and Y. Morimoto, Phys. Rev. B **62**, 5399 (2000).
[40] G. Matsumoto, J. Phys. Soc. Jpn. **29**, 615 (1970).
[41] D. N. Argyriou, J. F. Mitchell, C. D. Potter, D. G. Hinks, J. D. Jorgensen, and S. D. Bader, Phys. Rev. Lett. **76**, 3826 (1996).
[42] B. Dabrowski, K. Rogacki, X. Xiong, P. W. Klamut, R. Dybzinski, J. Shaffer, and J. D. Jorgensen, Phys. Rev. B **58**, 2716 (1998).
[43] N. F. Mott and E. A. Davis, *Electronic Processes in Non-Crystalline Materials* (Clarendon Press, Oxford, 1979), p. 31.
[44] D. Emin, C. H. Seager, and R. K. Quinn, Phys. Rev. Lett. **28**, 813 (1972).
[45] D. Emin, in *Science and Technology of Magnetic Oxides*, MRS Symp. Proc. No. 494, edited by M. F. Hundley, J. H. Nickel, R. Ramesh, and Y. Tokura (Materials Research Society, Warrendale, 1998), p. 163.